Influence of the potential range on the heat capacity of 13-atom Morse clusters

Michael Moseler
School of Physics, Georgia Institute of Technology, 837 State Street, Atlanta, Georgia 30332

Johannes Nordiek
Freiburger Materialforschungszentrum, Stefan-Meier-Strasse 21, 79104 Freiburg, Germany

(Received 5 May 1999)

Heat capacity curves as a function of temperature were studied for 13-atom clusters bound by Morse potentials with different range parameters $\rho_0 \in \{3,4,5,6,14\}$ using J-walking Monte Carlo. Decreasing the range of the pair potential (i.e., increasing ρ_0) increases the peak of the heat capacity in the melting transition region and decreases the boiling temperature. For $\rho_0 = 14$ the melting and boiling peaks merge. The short-range potential favors a transition from the catchment region of the icosahedral ground state to the basins of higher minima. On the other hand, clusters bound by the long-range potential ($\rho_0 = 3$) remain in the ground-state basin even for elevated temperatures, which can be explained by the destabilization of important higher minima for $\rho_0 < 4$. [S0163-1829(99)08839-6]

I. INTRODUCTION

In a recent experiment the caloric curves $E(T)$ and heat capacities of free sodium clusters have been determined.[1] A peak of $C(T)$ occurring at a temperature below the melting temperature of bulk sodium was interpreted as the melting transition of the finite system. Such a phase change in small clusters has been predicted by computer simulations more than ten years ago.[2] It was shown by Jellinek, Beck, and Berry that small Lennard-Jones clusters may appear in two distinct forms with properties reminiscent of the solid and liquid phases of bulk matter, respectively, and that these two forms can coexist dynamically over a finite temperature range starting with a freezing temperature T_f and ending with a melting temperature T_m. Consequently, for temperatures between T_m and T_f the potential energy distribution is bimodal, and therefore has a larger standard deviation leading to a peak in $C(T)$.

However, such bimodality is greatly affected by the shape of the potential energy surface (PES) applied in the simulation. Mainz and Berry[3] studied the molecular dynamic (MD) trajectories of seven-atom clusters bound by a pairwise additive Morse potential. They demonstrated that an increase of the potential range can drastically reduce coexistence. The influence of the range of the potential on purely thermodynamic properties like the heat capacity has been studied by Rey and co-workers. Strengthening the repulsion of a Lennard-Jones potential (i.e., reducing the potential range) resulted in an enhanced melting peak.[4] On the other hand, the melting peak vanished when the range of the attractive part of a hard core Yukawa potential was decreased.[5] However, these latter findings cannot be explained in terms of the presence or absence of coexistence, because sublimation takes place before melting, merging the melting and boiling peaks.

The present study aims on a deeper understanding of how the PES influences the $C(T)$ curve. Though more realistic many-body potentials for metals like sodium are available,[6,7] we decided to employ a PES formed by pairwise additive potentials, in order to deal with as few parameters as possible. More specifically, we chose the Morse potential which after renormalization of length and energy has only one free parameter. This parameter determines the range of the potential and can be adjusted in order to describe qualitatively a variety of materials such as alkali metals, transition metals, or noble gases.[8]

We have performed extensive J-walk Monte Carlo simulations for 13-atom clusters. For very long-ranged potentials, the melting peak nearly vanished in agreement with the observed reduction of coexistence.[3] We can characterize the PES by a set of local minima and a trajectory by the dwell probability in their basins.[9] In order to gain further insight into the interrelation between the PES-morphology and the thermodynamic behavior we separated the histogram of potential energies into two parts, the first one accumulating only configurations belonging to the catchment region of the absolute minimum and the second one accumulating all other configurations. Analyzing these two parts separately allowed us to identify two distinct origins of a heat-capacity peak.

II. COMPUTATIONAL METHOD

The PES of the N-atom Morse cluster (in this study $N = 13$) is given by

$$V(\mathbf{r}_1, \ldots \mathbf{r}_N) = \sum_{i<j} \epsilon e^{\rho_0(r_{ij}/r_e - 1)}(e^{\rho_0(r_{ij}/r_e - 1)} - 2). \quad (1)$$

In the following, energies and distances are measured in reduced units, i.e., the well depth ϵ and the equilibrium separation r_e are set to unity. The parameter ρ_0 determines the range of the potential. For metals rather long ranges with ρ_0 between about 3 and 5 are applied,[10] the shorter range of rare gases may be modeled by $\rho_0 = 6$, and the Girifalco potential for C_{60} can be approximated by a Morse potential with $\rho_0 \approx 14$.[11] Therefore, in the following calculations the range parameter was chosen to be 3, 4, and 5. For a comparison of metals with other materials the cases $\rho_0 = 6$ and 14 were studied, too. In order to reflect evaporated atoms back to the

cluster, the system was enclosed within a spherical container of radius $R=4$ centered on the cluster's center of mass.

Cluster heat capacities were calculated using the J-walking Monte Carlo method[12] which, compared to ordinary Metropolis Monte Carlo, reduces substantially errors caused by incomplete sampling of configurational space. Large barriers can be more easily surmounted with this method. In our J-walking calculations Monte Carlo trajectories for three different temperatures $1/\beta_1 > 1/\beta_2 > 1/\beta_3$ were generated. Each trajectory consisted of 5×10^5 warmup sweeps followed by 2×10^6 sweeps of data accumulation. Every tenth sweep the cluster configuration $\mathbf{r}=(\mathbf{r}_1,\ldots\mathbf{r}_N)$ was recorded forming a sample

$$\mathbf{r}_{\beta_j}^{(i)}(i=1,\ldots,200\,000,\ \ j=1,\ldots,3) \tag{2}$$

of the Boltzmann distribution. For the high-temperature trajectory standard Metropolis sampling was used,[13] where the maximum displacement of an atom was adjusted to yield a move acceptance of about 50%. The temperature $1/\beta_1$ was chosen to be 0.5 reduced units (i.e., $k_B=1$). This is well above the melting temperature and therefore barrier crossing occurs frequently enough. However, at the lower temperature $1/\beta_2$ a Metropolis Monte Carlo trajectory may be trapped in the catchment region of a local minimum. In order to avoid such a nonergodic walk, jumps to a randomly selected configuration of the $\mathbf{r}_{\beta_1}^{(i)}$ distribution were attempted every move with a propability $P_J=0.1$. In order to guarantee detailed balance of this jump-walk, the acceptance probability for the jump from $\mathbf{r}$ to $\mathbf{r}_{\beta_1}^{(i)}$ was given by

$$p=\min(1,\exp\{(\beta_1-\beta_2)[V(\mathbf{r}_{\beta_1}^{(i)})-V(\mathbf{r})]\}). \tag{3}$$

These frequent jumps encourage trajectories to overcome barriers and thus increase the convergence of the heat-capacity results. The inverse temperature β_2 was automatically adjusted to yield a 10% acceptance of the attempted jumps. This ensures a sufficient overlapping of the two energy distributions. The whole procedure was repeated for a J walk at the third temperature $1/\beta_3 < 1/\beta_2$, where now jumps to the β_2 configurations were attempted. This temperature was low enough allowing the walk to sample the solid phase of the cluster.

The results of a J-walk depend slightly on the starting configuration of the high-temperature walk.[14] Therefore, for every range parameter ρ_0 four J-walk chains

$$(\beta_1,\beta_2,\beta_3) \tag{4}$$

with different random starting configurations for the β_1 walk were calculated. Due to their automatic determination, the temperatures $1/\beta_2$ and $1/\beta_3$ are slightly different in the individual J-walk chains. Typical values for the case of $\rho_0=3$ are $1/\beta_2=0.29$ and $1/\beta_3=0.18$. For $\rho_0=14$, on the other hand, one has $1/\beta_2=0.31$ and $1/\beta_3=0.24$. The resulting 12 histograms for every ρ_0 have been analyzed using the multiple histogram method,[15] providing the configurational entropy $S(E)=\ln\Omega(E)$ as a function of potential energy E with the configurational density of states

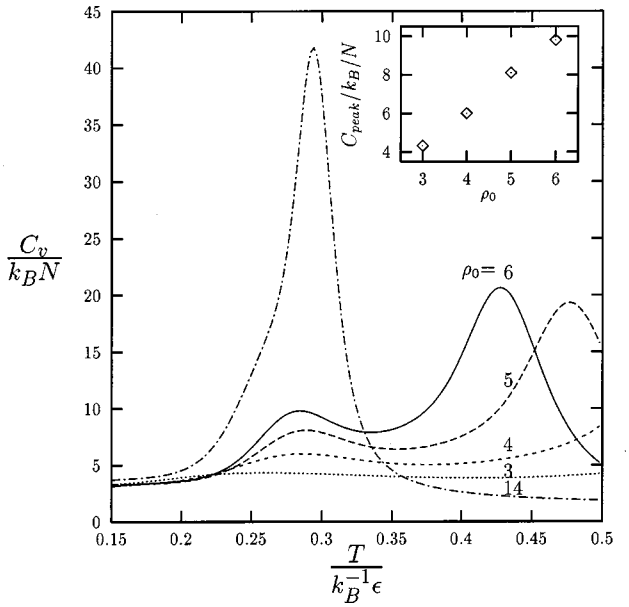

FIG. 1. Heat-capacity curves of a $N=13$ Morse cluster as a function of temperature. The inset displays a nearly linear dependence of the maximum near $T=0.3\epsilon/k_B$ on the range parameter ρ_0.

$$\Omega(E)=\int d^{3N}r\,\delta(V(\mathbf{r})-E). \tag{5}$$

It is also useful to calculate the entropy from each of the 12 histograms alone. Wherever two or more of the histograms are overlapping, they should yield (up to an additive constant) the same entropy curves. This offers a thorough test of the consistency of the histograms.

The canonical constant volume heat capacity was computed by

$$C_v(T)=\frac{1}{T^2}\left[\int dE\,E^2 f_\beta(E)-\left(\int dE\,E f_\beta(E)\right)^2\right]+\frac{3}{2}N, \tag{6}$$

where the potential-energy distribution is given by

$$f_\beta(E)=e^{(S(E)-\beta E)}\Big/\int dE' e^{[S(E')-\beta E']}. \tag{7}$$

III. RESULTS

Figure 1 shows the heat-capacity curves for the different potential ranges. For a range parameter $\rho_0\leqslant 6$ a solid-liquid transition peak occurs between $T=0.25$ and 0.3. The height of this peak is roughly a linear function of ρ_0 as indicated in the inset of Fig. 1. For $\rho_0=5$ and 6 a second peak associated with the boiling of the cluster is perceptible. Decreasing the potential range lowers the boiling temperature. For the very-short-ranged potential with $\rho_0=14$ melting and boiling coincide. One may consider the shoulder on the right-hand side of the boiling peak as a remainder of the melting peak.

The interrelation of the PES morphology and the thermodynamic behavior can be further analyzed by a basin map $B(\mathbf{r})$, which determines (by conjugate-gradient minimization) for each configuration $\mathbf{r}$ the local energy minimum to which it belongs. The set of all configurations associated in

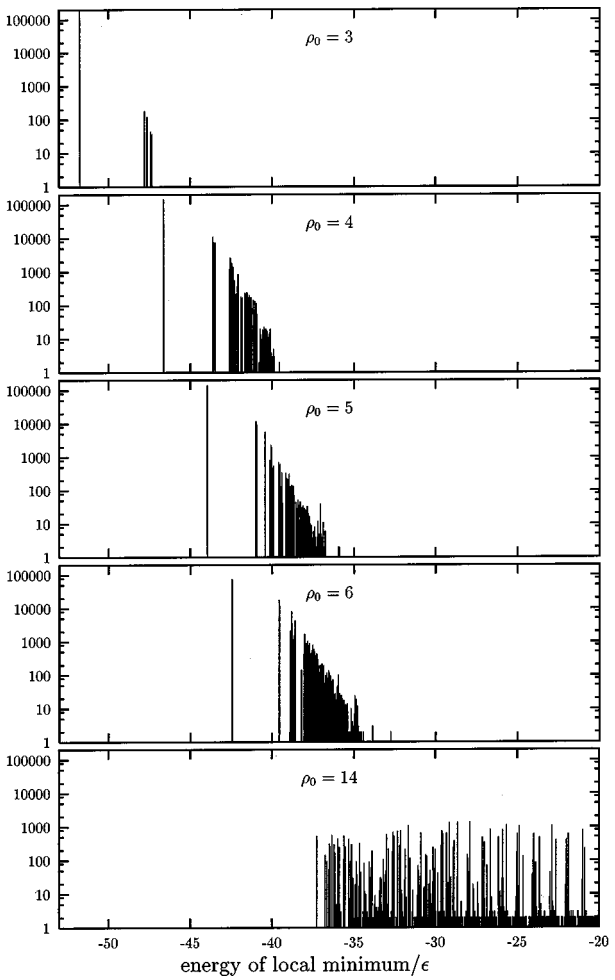

FIG. 2. Frequencies of occurrence of configurations belonging to different catchment areas at $T \approx 0.3\epsilon/k_B$. The horizontal axis displays the energy of the respective local minimum. The large needle on the left-hand side corresponds to the global minimum.

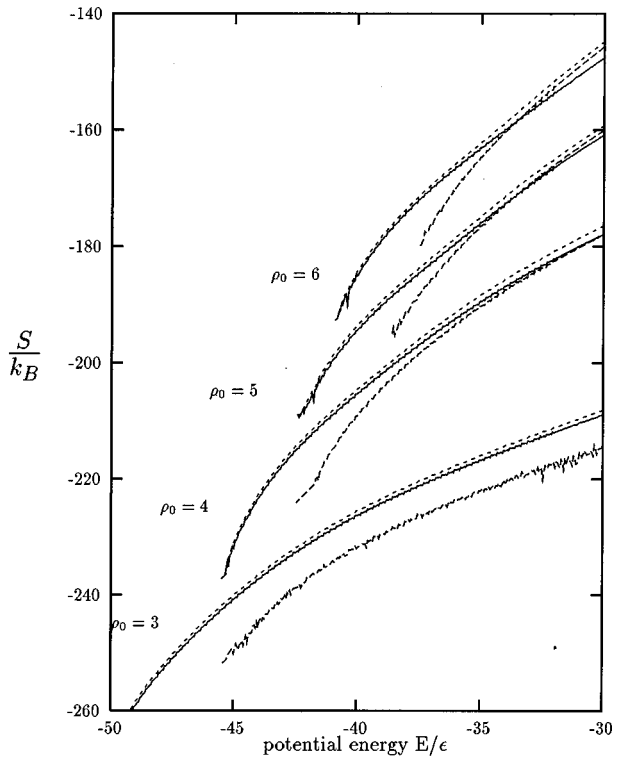

FIG. 3. Configurational entropy as a function of potential energy for the different range parameters ρ_0. The solid curves represent the entropy of the global minimum basin $S_1(E)$ and the long-dashed curves the entropy $S_2(E)$ of the higher minima basins. For the definition of S_1 and S_2 see text. The total configurational entropies are given by short dashes.

this way with a certain minimum is called its basin (or its catchment region).

For the distributions $\mathbf{r}_{\beta_j}^{(i)}$ we have calculated histograms of the local minimum energies $B(\mathbf{r}_{\beta_j}^{(i)})$ by the conjugate gradient method.[16] An inspection of the frequencies of the global minimum (the icosahedron) and the other local minima proved to be very useful for an explanation of the differences in the $C_v(T)$ curves (Fig. 2). The clusters with $\rho_0 > 3$ frequently visit higher states at elevated temperatures, as expected. However, the $\rho_0 = 3$ cluster remains almost completely in the catchment region of the icosahedron. Thus obviously the part of the configuration space occupied by the catchment region of the icosahedron becomes the more dominant the larger the range of the potential (i.e., the lower ρ_0) is.

This trend is additionally increased by the destabilization of the three most important higher minima, which are icosahedra with one particle plucked out and put onto three different locations on the surface. These minima became unstable for values of $\rho_0 < 4$ leading to the qualitative differences between $\rho_0 = 3$ and 4 in Fig. 2, including the larger energy gap between the absolute minimum and the higher minima for $\rho_0 = 3$. Comparing these observations with the heat capacity curves (Fig. 1) it becomes evident that mainly the proportion of the configuration space belonging to the higher minima determines the height of the heat capacity peak.

This conjecture can be stated more precisely in the following way. Let us split the density of states into two contributions: the density of states in the catchment basin of the ground state

$$\Omega_1(E) = \int_{B(\mathbf{r}) = E_{ico}} d^{3N} r \, \delta(V(\mathbf{r}) - E) \tag{8}$$

and the remaining part $\Omega_2(E) = \Omega(E) - \Omega_1(E)$ belonging to the higher local minima. Splitting the histograms analogously and then applying the multiple histogram method we gain the two entropies $S_1(E) = \ln \Omega_1(E)$ and $S_2(E) = \ln \Omega_2(E)$. In Fig. 3 they are depicted together with the total entropy

$$S(E) = \ln[\Omega_1(E) + \Omega_2(E)]. \tag{9}$$

Two different types of behavior can be observed. They become most clearly, if one compares the cases, $\rho_0 = 3$ and $\rho_0 = 6$. At $\rho_0 = 3$, S_2 is always less than S_1. That means, in accordance with our previous observation, that at any temperature only states from the basin of the icosahedron make a perceptible contribution to the partition function. Thus the heat-capacity peak, which is very small in this case (see Fig. 1), originates from the anharmonicity of the icosahedron's

catchment region alone. The presence of further minima has no perceptible influence in this case.

The situation is different at $\rho_0=6$. In this case there exists an intersection of the two curves $S_1(E)$ and $S_2(E)$ at $E \approx -33$. This intersection leads to a segment of positive curvature in the total entropy and thus to a heat capacity peak. That means that in this case the thermodynamic behavior can be interpreted in terms of a two-state model. Each of the two parts of the distribution function represents a different thermodynamic state with its own entropy and its own thermodynamic functions. The behavior of the system as a whole results from a mixture of these two thermodynamic states. It is true, that a slightly positive curvature occurs in S_1 alone, and so the low-energy phase should not be called a purely solid phase. But by far the most important contribution to the characteristic feature of $S(E)$ originates from the combination of S_1 and S_2 according to Eq. (9). That is proven in Fig. 4, which shows for $\rho_0=6$ the heat capacities as calculated from S_1, S_2, and S. The total heat capacity is not predictable from the two partial heat capacities alone. Thus here, in opposition to the case $\rho_0=3$, the heat-capacity peak is due to the fact that above a certain threshold temperature the cluster can assume a great number of excited structures corresponding to a sudden increase of available configuration space.

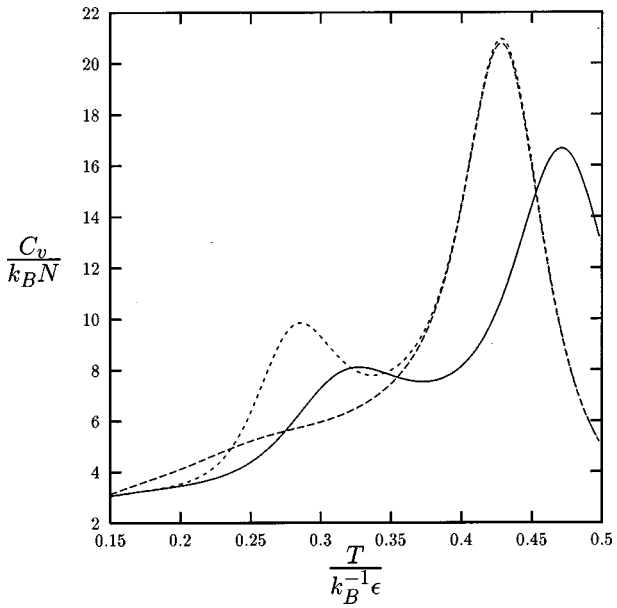

FIG. 4. Heat-capacity curves for $\rho_0=6$. Solid curve: $C_v(T)$ calculated from the entropy S_1 of the ground-state basin; long dashes: $C_v(T)$ determined by entropy S_2 of higher-energy basins; short dashes: total heat capacity.

IV. CONCLUSION

In the present paper we found an anticorrelation between the height of the melting heat-capacity peak of a 13-atom Morse cluster and the range of the interatomic potential. This effect can be explained in terms of the distribution of configuration space among the different catchment regions. A sizable heat-capacity peak occurs, when at a certain temperature a remarkable amount of configuration space belonging to the catchment regions of higher minima becomes available. This is the case for rather short-ranged potentials ($\rho_0=6$). For the longer-ranged potentials ($\rho_0=3$) the largest part of configuration space belongs to the catchment region of the absolute minimum and the great majority of configurations remains there even at elevated temperatures. Nevertheless a small peak is observable in this case, too. This could be due to transition states joining different permutational ground-state isomers or due to saddles between the ground-state and a small number of higher local minima.

Despite the simplicity of the Morse PES a few conclusions concerning real materials can be drawn from our results: Since metal potentials exhibit generally a larger range than for instance rare gases, our results suggest smaller heat-capacity peaks for metal clusters compared to the pronounced peaks in Lennard-Jones clusters. Furthermore, the observed lowering of the boiling point with increasing ρ_0 is consistent with the narrow temperature range in which melting and boiling of bulk rare gases occur. However, in order to interprete experimentally measured $C(T)$ curves in more detail, further studies for a variety of cluster sizes and using more flexible potentials will be necessary. Hopefully, this will provide a more systematic understanding of the relation between the PES morphology and the heat-capacity curve.

[1] M. Schmidt, R. Kusche, W. Kronmüller, B. von Issendorff, and H. Haberland, Phys. Rev. Lett. **79**, 99 (1997); M. Schmidt, R. Kusche, B. von Issendorff, and H. Haberland, Nature **393**, 238 (1998).
[2] J. Jellinek, T.L. Beck, and R.S. Berry, J. Chem. Phys. **84**, 2783 (1986).
[3] D. Mainz and S. Berry, Mol. Phys. **88**, 709 (1996).
[4] C. Rey, J. Garcia-Rodeja, L.J. Gallego, and M.J. Grimson, Phys. Rev. E **57**, 4420 (1998).
[5] C. Rey and L.J. Gallego, Phys. Rev. E **53**, 2480 (1996).
[6] Y. Li, E. Blaisten-Barojas, and D.A. Papaconstantopoulus, Phys. Rev. B **57**, 15 519 (1998).
[7] R. Poteau and F. Spiegelmann, Phys. Rev. B **45**, 1878 (1992).
[8] J. Doye and D. Wales, J. Chem. Soc., Faraday Trans. **93**, 4233 (1997).
[9] F.G. Amar and R.S. Berry, J. Chem. Phys. **85**, 5943 (1986).
[10] L.A. Girifalco and V.G. Weizer, Phys. Rev. **114**, 687 (1959).
[11] J. Doye and D. Wales, J. Chem. Soc., Faraday Trans. **90**, 1061 (1994).
[12] D.D. Frantz, J. Chem. Phys. **102**, 3747 (1995).
[13] N. Metropolis, M. Rosenbluth, M.N. Rosenbluth, A. Teller, and E. Teller, J. Chem. Phys. **21**, 1087 (1953).
[14] D.D. Frantz, J. Chem. Phys. **105**, 10 030 (1996).
[15] A.M. Ferrenberg and R.H. Swendsen, Phys. Rev. Lett. **63**, 1195 (1989).
[16] W.H. Press, S.A. Teukolsky, W.T. Vetterling, and B.P. Flannery, *Numerical Recipes* (Cambridge University Press, Cambridge, 1986).